Civil Engineering Dimension
https://ced.petra.ac.id

Scour Development in Square Pile Groups: Effects of Pile Number and Spacing

Puspasari, A.D.[1]* and Tang, J.-H.[2]
[1] Department of Civil Engineering, Institut Teknologi Adhi Tama Surabaya
Jl. Arief Rahman Hakim No. 100, 60117 Surabaya, East Java, INDONESIA
[2] Department of Civil Engineering, Chung Yuan Christian University
200 Chung Pei Road, Chung Li District, Taoyuan City 320, TAIWAN

DOI: https://doi.org/10.9744/ced.28.2.276-290

Article Info:
Submitted: Nov 25, 2025
Reviewed: Mar 11, 2026
Accepted: July 28, 2026

Keywords:
local scour,
pile group,
square configuration,
numerical simulation,
CFD,
flow-3D.

Corresponding Author:
Puspasari, A.D.
Department of Civil Engineering,
Institut Teknologi Adhi Tama Surabaya
Jl. Arief Rahman Hakim No. 100, 60117
Surabaya, East Java, INDONESIA
Email: aisyahdwipus@itats.ac.id

Abstract

Local scour around pile group foundations poses a significant risk to hydraulic and coastal structures, particularly when multiple piles interact with complex flow patterns. This study presents a numerical investigation of local scour around pile groups arranged in 2×2, 3×3, and 4×4 square configurations using Flow-3D. The model incorporates clear-water scour conditions, the RNG k–ε turbulence scheme, FAVOR geometry representation, and the Van Rijn sediment transport formulation. Simulations were conducted for three pile spacing ratios (G/D = 2.5, 3, 3.5) to evaluate the influence of pile number and spacing on scour depth and scour-hole morphology. The results show that scour decreases from upstream to downstream piles due to sheltering, while central piles experience slightly deeper scour due to intensified flow interference. Increasing spacing reduces pile-to-pile interaction and leads to scour patterns resembling single-pile behavior. Overall, the numerical model reliably captures scour mechanisms and provides useful insights for safer pile-group design.

INTRODUCTION

Pile foundations are widely used in the construction of bridge piers and offshore structures due to their ability to transfer structural loads to deeper, more stable soil strata [1]. However, one of the most persistent and critical challenges in hydraulic engineering is local scour, in which flowing water erodes sediment around pile foundations, compromising structural stability [2]. Catastrophic failures such as the Schoharie Creek Bridge collapse in the United States [3] and the Houfeng Bridge in Taiwan [4] have highlighted the potentially devastating consequences of scour-induced failures, including loss of life, economic disruption, and environmental damage.

Local scour is initiated by the disturbance of flow patterns around pile foundations, which induces high shear stress and turbulent structures such as horseshoe and wake vortices. These complex flow mechanisms entrain and transport bed sediments, progressively deepening the scour hole around and between piles. While the mechanisms of scour around isolated pile are relatively well understood, the presence of multiple piles in a group arrangement significantly alters the flow field pile–pile interactions, leading to more complex and unpredictable scour behavior [5].

Recent advancements in Computational Fluid Dynamics (CFD) have enabled more accurate simulations of sediment transport and scour evolution under varying hydraulic conditions [6]. Flow-3D, a CFD software incorporating the

Note : Discussion is expected before November, 1st 2026, and will be published in the “Civil Engineering Dimension”, volume 29, number 1, March 2027.
ISSN : 1410-9530 print / 1979-570X online
Published by : **Petra Christian University**

Volume of Fluid (VOF) and FAVOR methods, has been successfully applied in previous studies to model scour phenomena around cylindrical piles with good agreement to experimental data [7]. The use of the RNG k–ε turbulence model and Van Rijn sediment transport equation has been particularly effective in capturing the evolution of bed elevation and vortex structures around pile foundations.

To date, many numerical investigations have focused on pile groups arranged in linear (tandem) or side-by-side configurations. However, square configurations, which are commonly used in practical foundation design for their geometric efficiency and structural redundancy, have not been extensively studied. The lack of comprehensive insight into the scour dynamics of such arrangements presents a significant gap in current understanding, especially considering the mutual interference effects among multiple rows and columns of piles.

Abdeldayem et al. [8] investigated the scour depth around groups of four and nine piles arranged in a square configuration, considering transverse spacing ratios (ST/b) and longitudinal spacing ratios (SL/b) of 1, 2, 3, and 4. Their findings indicate that scour depth decreases as pile spacing increases, eventually approaching the scour depth observed for a single isolated pile when the spacing ratio reaches approximately 7.7 to 10.3. Furthermore, the study shows that transverse spacing has a more pronounced influence on scour depth than longitudinal spacing.

Wang et al. [9] simulated the scour depth around four piles arranged in a square configuration, using a pile diameter (D) of 0.03 m and a spacing ratio of 2D. The numerical model was set within a channel measuring 2.7 m in length, 0.8 m in width, and 1 m in height, with a constant inflow velocity of 22.5 cm/s and a water depth of 25 cm. The results indicate that the front piles experienced greater scour depths than the rear piles due to the shielding effect.

Previous studies have provided important insights into scour around pile groups; however, several limitations remain. Abdeldayem et al. [8] primarily focused on the influence of pile spacing without thoroughly addressing the spatial variation of scour and flow–sediment interaction within multi-row configurations. Similarly, Wang et al. [9] examined scour in a 2×2 arrangement with a single spacing ratio, limiting the understanding of pile–pile interaction in more complex and larger group configurations.

Therefore, in this study, a series of numerical simulations is conducted using Flow-3D to analyze the local scour characteristics around pile groups arranged in square configurations comprising 2×2, 3×3, and 4×4 cylindrical piles. Each configuration is evaluated under three different pile spacing ratios (G/D = 2.5, 3.0, and 3.5) to assess the influence of geometric parameters on maximum scour depth and scour pattern evolution. The aim is to provide a more comprehensive understanding of local scour mechanisms around square pile groups by analyzing key measurable parameters, including maximum scour depth and the temporal evolution of scour. In addition, flow interference and pile interaction effects are interpreted based on the spatial distribution and development of scour patterns under different pile configurations and spacing ratios. These findings are relevant to practical engineering design, and support the development of optimalstrategies tominimize scour risk in bridge and offshore foundation systems.

NUMERICAL METHOD

This study employed Flow-3D v11.2, a Computational Fluid Dynamics (CFD) software, to simulate the evolution of local scour around square pile groups. Flow-3D solves the three-dimensional Reynolds-Averaged Navier–Stokes (RANS) equations for incompressible flow, coupled with sediment transport and bed deformation models. The free-surface motion was captured using the Volume of Fluid (VOF) method, while the complex cylindrical geometry of piles was represented through the Fractional Area/Volume Obstacle Representation (FAVOR) technique, which allows accurate treatment of curved boundaries within a Cartesian grid.

The turbulence closure was achieved using the RNG k–ε model, which is widely recognized for its ability to represent low-intensity turbulent flows and regions with strong shear layers, providing a good balance between accuracy and computational efficiency. Sediment transport was modeled using the Van Rijn bed-load transport formulation [10], which has been demonstrated in previous studies to predict scour depth and bed evolution with good agreement to experimental data. The sediment was assumed to be uniform and non-cohesive, with properties defined by median grain size, density, angle of repose, and critical Shields parameter.

Three pile group configurations were examined in the present work: 2×2 (four piles), 3×3 (nine piles), and 4×4 (sixteen piles) arranged in square patterns. For each configuration, three pile spacing ratios were considered, with center-to-center spacing relative to pile diameter (G/D = 2.5, 3.0, and 3.5). The computational domain was designed to minimize boundary influences, with sufficient upstream length to allow flow development and downstream length to capture vortex shedding and sediment transport. Boundary conditions included a specified inflow velocity at the inlet, pressure outlet at the downstream boundary, rigid no-slip conditions along the bed and sidewalls, and a pressure boundary at the free surface.

A structured mesh was generated with local refinement around the pile groups to accurately resolve near-bed turbulence and sediment entrainment. Coarser grids were applied toward the far-field boundaries to optimize computational resources. Grid sensitivity checks were performed to ensure solution independence from mesh resolution. The time step was selected to satisfy numerical stability criteria while capturing the temporal evolution of the scour process.

To ensure the reliability of the numerical approach, the model was first validated against published experimental data for scour around a single pile. The validation was conducted by comparing the numerical and experimental results in terms of maximum scour depth temporal evolution of scour, and scour-hole morphology. Good agreement was observed for those parameters, thereby confirming the applicability of the present model for simulating scour in square pile group arrangements.

Governing Equations

The simulations were carried out using Flow-3D v11.2, a commercial Computational Fluid Dynamics (CFD) software package widely used in hydraulic and sediment transport studies. Flow-3D solves the Reynolds-Averaged Navier–Stokes (RANS) equations for incompressible turbulent flow, coupled with sediment transport and bed deformation models. The governing equations include the continuity equation, momentum conservation, and sediment transport formulations, expressed as:

$$\frac{\partial u}{\partial t} + \frac{1}{V_F}\left(uA_x\frac{\partial u}{\partial x} + vA_y\frac{\partial u}{\partial y} + wA_z\frac{\partial u}{\partial z}\right) = -\frac{1}{\rho}\frac{\partial p}{\partial x} + G_x + f_x, \tag{1}$$

$$\frac{\partial v}{\partial t} + \frac{1}{V_F}\left(uA_x\frac{\partial v}{\partial x} + vA_y\frac{\partial v}{\partial y} + wA_z\frac{\partial v}{\partial z}\right) = -\frac{1}{\rho}\frac{\partial p}{\partial y} + G_y + f_y, \tag{2}$$

$$\frac{\partial w}{\partial t} + \frac{1}{V_F}\left(uA_x\frac{\partial w}{\partial x} + vA_y\frac{\partial w}{\partial y} + wA_z\frac{\partial w}{\partial z}\right) = -\frac{1}{\rho}\frac{\partial p}{\partial z} + G_z + f_z. \tag{3}$$

where V_F and A_i represent the volume fraction and area fraction, respectively; ρ and p denote the fluid density and the average hydrodynamic pressure; and G_i and f_i correspond to the body acceleration and viscous acceleration.

Turbulence Model

Turbulence closure was achieved using the Renormalization Group (RNG) k–ε model, which provides improved accuracy in low-intensity turbulent flows and regions with high strain rates compared to the standard k–ε model. The RNG k–ε model has been widely adopted in scour simulations due to its balance of precision and computational efficiency.

$$\frac{\partial k_T}{\partial t} + \frac{1}{V_F}\left\{uA_x\frac{\partial k_T}{\partial x} + vA_y\frac{\partial k_T}{\partial y} + wA_z\frac{\partial k_T}{\partial z}\right\} = P_T + G_T + Diff_{k_T} - \varepsilon_T, \tag{4}$$

$$\frac{\partial k_T}{\partial t} + \frac{1}{V_F}\left\{uA_x\frac{\partial k_T}{\partial x} + vA_y\frac{\partial k_T}{\partial y} + wA_z\frac{\partial k_T}{\partial z}\right\} = \frac{CDIS1\,.\,\varepsilon_T}{k_T}(P_T + CDIS3\,.\,G_T) + Diff_\varepsilon - CDIS2\frac{\varepsilon^2{}_T}{k_T}. \tag{5}$$

where k_T is the turbulent kinetic energy associated with flow variations caused by fluctuating velocities; V_F, A_x, A_y, and A_z are the FAVOR functions in Flow-3D; P_T and G_T represent the production of turbulent kinetic energy and turbulent buoyancy. $Diff_{k_T}$ and $Diff_\varepsilon$ denote the diffusion terms of turbulent kinetic energy and dissipation, while ε_T is the turbulent energy dissipation rate. *CDIS1*, *CDIS2*, and *CDIS3* are the coefficients for production, decay, and buoyancy, respectively, and are user-adjustable dimensionless parameters with default values of 1.44, 1.92, and 0.2.

Sediment Scour Model

Sediment motion was simulated using the Van Rijn bed-load transport equation [10], which calculates sediment entrainment, transport, and deposition. This equation has been shown to yield reliable predictions of scour depth and time evolution in local scour studies around piles. The sediment properties considered in this study included median particle diameter (d50), density, repose angle, and shields parameter. The bed deformation was updated dynamically to account for erosion and deposition processes, enabling simulation of scour-hole evolution.

$$\Phi_i = \beta_{VR,i}\, d_{*,i}^{\;-0.3} \left(\frac{\theta_i}{\theta'_{cr,i}} - 1.0\right)^{2.1} c_{b,i}. \tag{6}$$

where $\beta_{VR,i}$ refers to the bed-load coefficient with a default value of 0.053, and $c_{b,i}$ denotes the volume fraction of species i within the bed material.

Meshing

A structured Cartesian mesh was employed, with refinement zones around the pile groups to capture detailed flow structures and sediment-bed interactions. Grid independence tests were performed to ensure that simulation results were not sensitive to further mesh refinement. The mesh configuration ensured that the cell aspect ratio (x:y:z) did not exceed 3:1 in any two directions, the ratio between adjacent cells (x:x, y:y, or z:z) was kept below 1.25 in the same direction, and the mesh transition between blocks (nested or linked) did not surpass 2:1 [11]. The mesh was gradually coarsened away from the pile groups to reduce computational cost while maintaining accuracy near critical regions.

Boundary Conditions

The computational domain was designed to minimize boundary effects, with adequate length upstream and downstream of the pile groups. The following boundary conditions were applied:

a. Inlet: uniform velocity specified to represent clear-water scour conditions.
b. Outlet: outflow boundary to allow free passage of water and sediment.
c. Top boundary: specified pressure boundary to represent the free surface.
d. Bottom and sidewalls: rigid wall with no-slip condition.

The free surface flow was tracked using the Volume of Fluid (VOF) method, while complex geometries such as cylindrical piles were resolved using the Fractional Area/Volume Obstacle Representation (FAVOR) method.

NUMERICAL SIMULATION OF SQUARE PILE CONFIGURATIONS

Before the numerical simulations of local scour around square pile configurations were carried out, validation of the experimental and numerical models was first conducted. In this study, model verification was performed through a single-pile scour test, in which the numerical predictions were evaluated against the experimental measurements reported by Khosronejad et al. [12].

Validation Model

The numerical model was configured to match the physical experiment, including its geometry and sediment properties. The flow channel used in the setup measured 10 m in length, 1.21 m in width, and 0.45 m in height. A cylindrical pile with a 0.1651 m diameter was positioned 4 m from the inlet. The sediment had a median grain size (d_{50}) of 0.00085 m within a 0.2-m layer, and the flow condition involved water moving at 0.25 m/s with a depth of 0.186 m The schematic diagrams of the numerical model and computational setup are presented in Figures 1–4. Several grid independence tests were performed to assess the mesh sensitivity of the numerical model, as shown in Figure 5. The selected mesh consisted of approximately 400,000 cells (400 × 50 × 20 in the x-, y-, and z-directions, respectively), with maximum adjacent cell size ratios of 1.1, 1.2, and 1.0 in the corresponding directions. This mesh provided a good balance between numerical accuracy and computational efficiency and produced scour depths that most closely matched the experimental results.

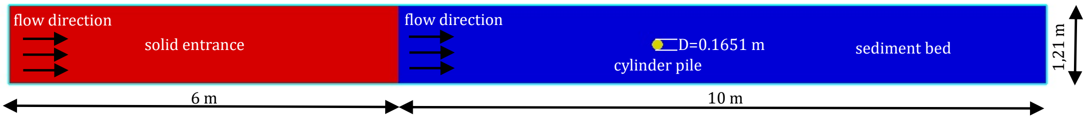

(a)

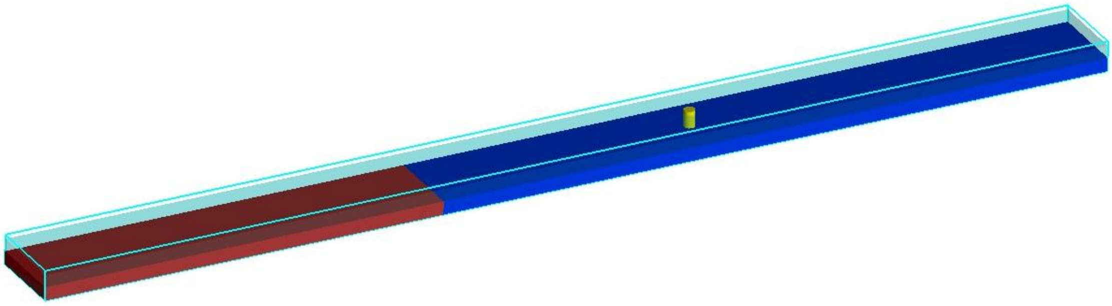

(b)

Figure 1. Schematic Diagram of the Validation Model: (a) Top View, (b) 3D View

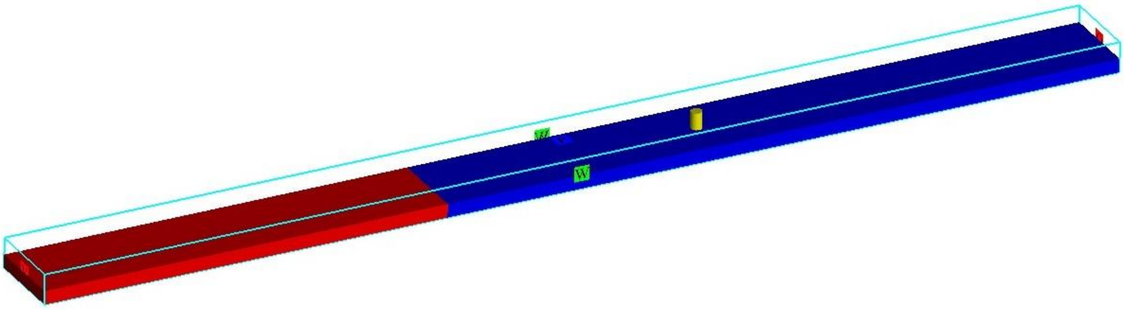

Figure 2. Schematic Diagram of Boundary Conditions

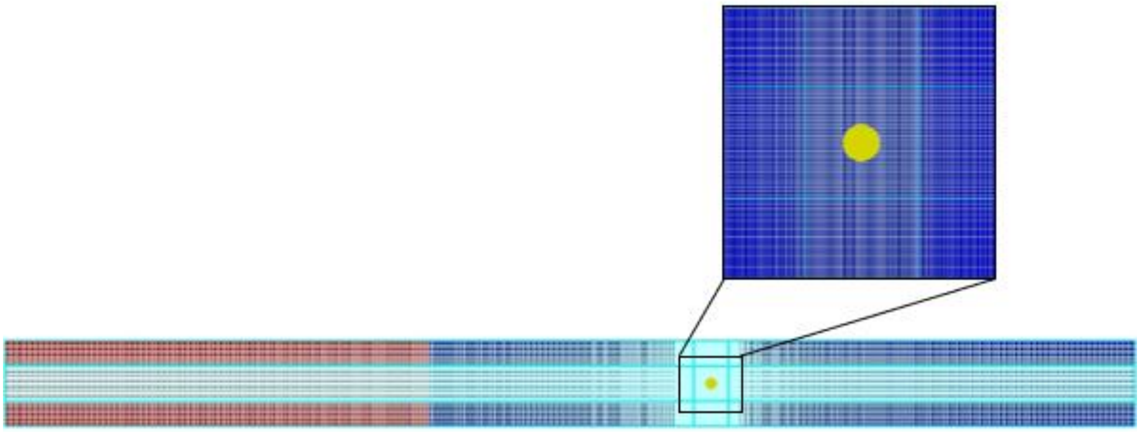

(a)

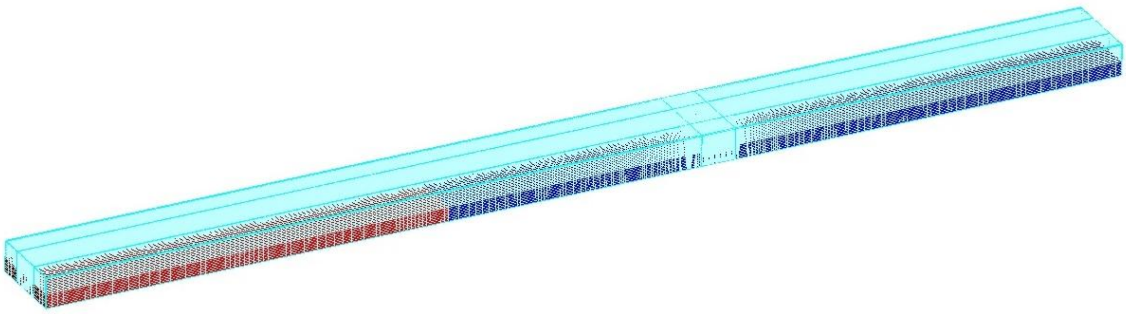

(b)

Figure 3. Schematic Diagram of Mesh Configuration: (a) Top View, (B) 3D View

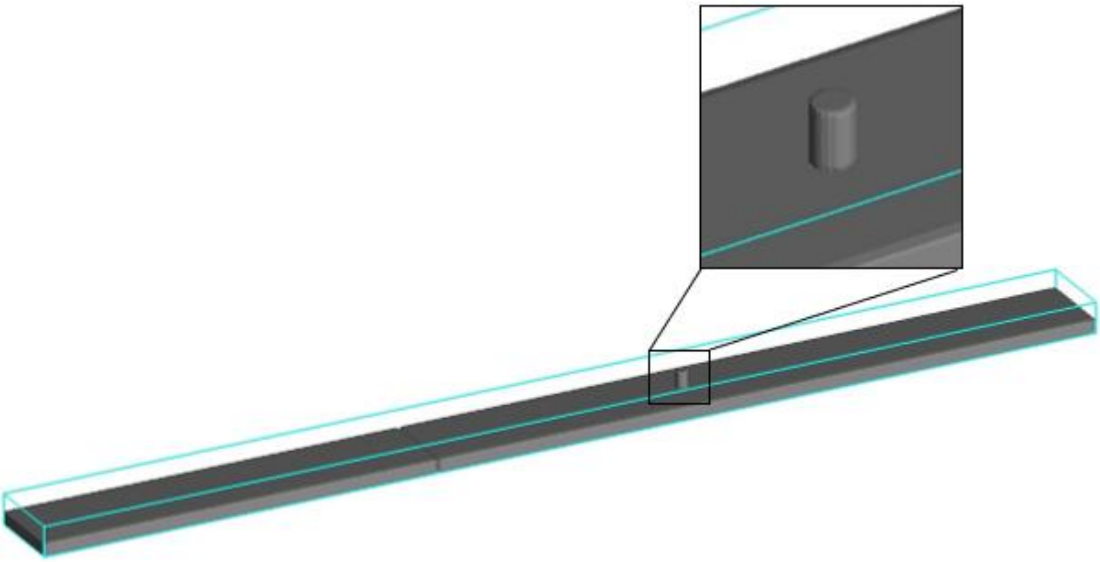

Figure 4. Schematic Diagram of FAVORize Model

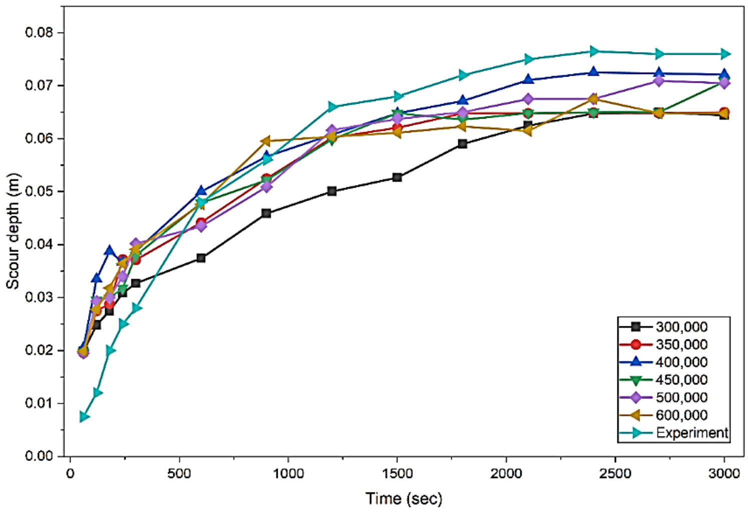

Figure 5. Grid Independence Test for Mesh Selection

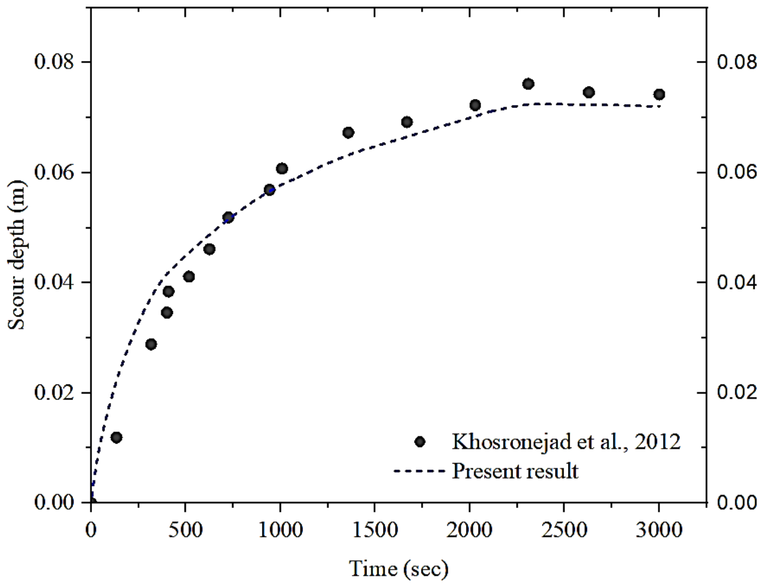

Figure 6. Time Evolution of Maximum Scour Depth, Modified from Tang and Puspasari [13]

As shown in Figure 6, after running the simulation for 3000 s until the scour depth stabilized, both the experimental and numerical results reached an equilibrium state, with final scour depths of 0.0742 m and 0.0721 m, respectively. During the experiment, however, the maximum scour depth observed at 2280 s was 0.0762 m slightly higher than the 0.0725 m predicted by the numerical model at the same time. The scour-depth progression shows that most of the erosion occurred within the first 1200 s. Interestingly, within the first 960 s, the numerical model produced a deeper scour than the experiment, but later the simulated depth became slightly shallower than the experimental measurements for the remainder of the test.

The higher predicted scour depth observed during the early stage (up to approximately 1000 s) can be attributed to rapid sediment entrainment under idealized numerical conditions. In contrast, the experimental results show a delayed initial response due to sediment packing effects and gradual turbulence development. As time progresses, the scour rate in the numerical model decreases and approaches equilibrium, whereas the experimental scour continues to evolve due to sustained vortex activity, resulting in the observed reversal trend.

The mechanism of local scour around the pile foundation is illustrated in Figure 7, showing its progression from the initial condition at t = 0 s to the equilibrium stage at t = 3000 s. The streamline patterns represent the flow motion and provide insight into the development of the local scour process.

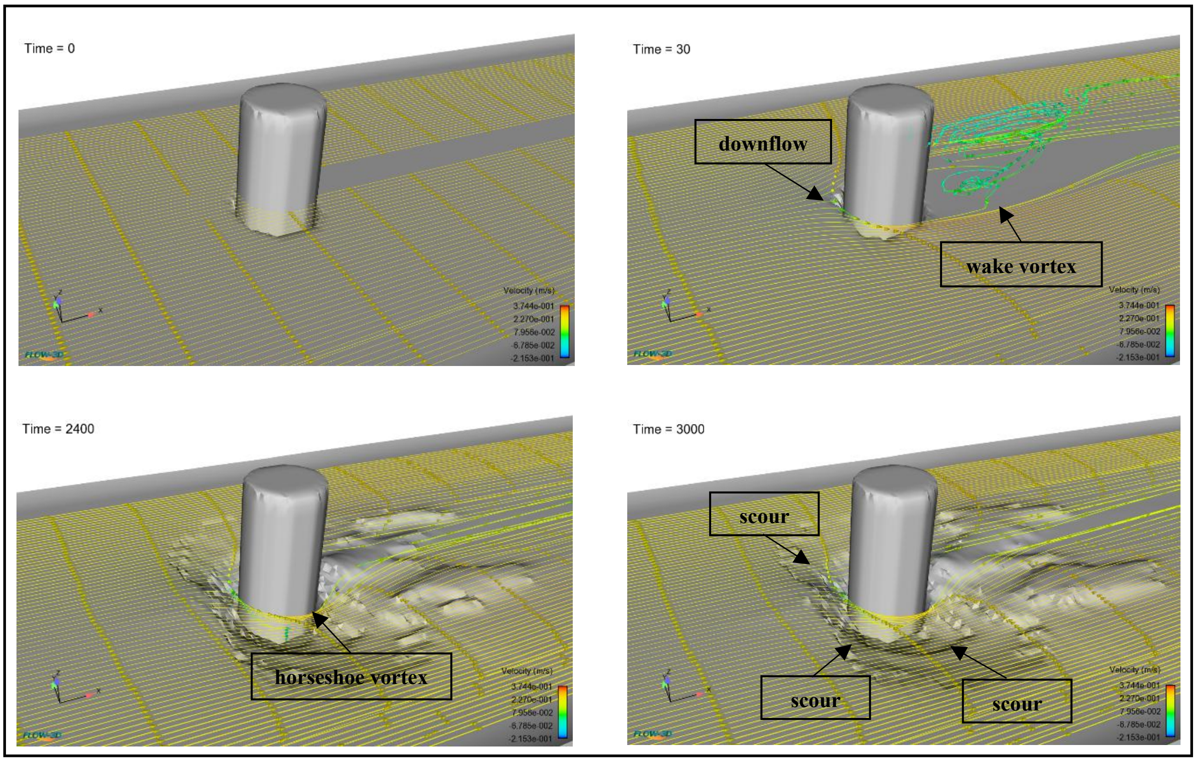

Figure 7. Temporal Evolution of Sediment Scour Mechanism

The flow approaching the cylindrical pile undergoes a change in direction upon obstruction, causing the incoming velocity to deflect downward into a vertical plane, forming a downflow driven by a pressure gradient. This downflow subsequently generates a horseshoe vortex in front of the pile, which plays a key role in initiating and intensifying local scour. In addition, flow acceleration around the pile increases the bed shear stress beyond the critical threshold, resulting in the entrainment and removal of sediment particles. Behind the pile, a wake vortex resembling a miniature tornado develops due to flow separation and lateral acceleration around the cylinder, as observed at t = 30 s, which over time contributes to sediment deposition. Furthermore, Figure 8 presents a comparison between the present numerical results and experimental data for local scour around a single pile in terms of bed elevation contours at the equilibrium stage [12].

The residuals between the numerical and experimental scour depths throughout the simulation are illustrated in Figure 9. Most residual values fall within the ±0.005 m tolerance range, indicating good overall agreement between the numerical and experimental results. In the early stages (approximately 400–600 s), the residuals are predominantly negative, indicating that the numerical model initially overpredicts the scour depth compared with the experiment. Between approximately 1000 and 1500 s, the residuals shift to positive values as the experimental scour depth slightly exceeds the numerical prediction. After 2000 s, the residuals gradually converge toward zero, reflecting the stabilization of scour development and the approach to equilibrium conditions in both datasets.

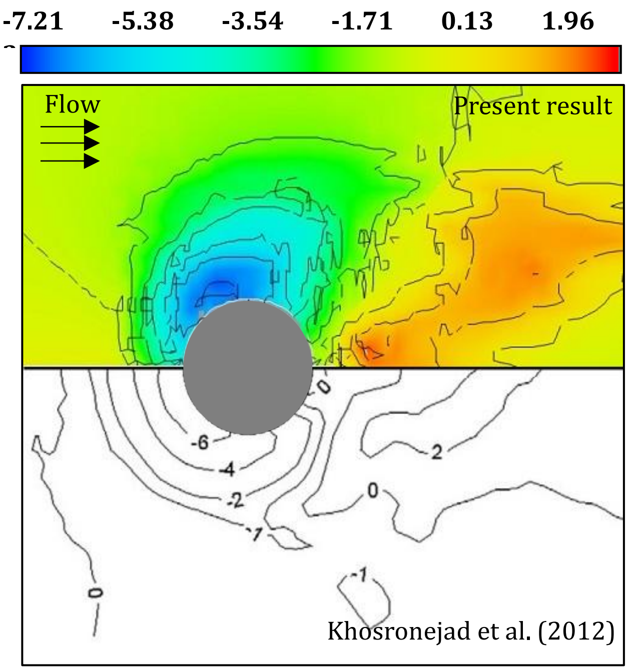

Figure 8. Comparison of Scour Pattern around A Single Pile, Modified from Tang and Puspasari [13]

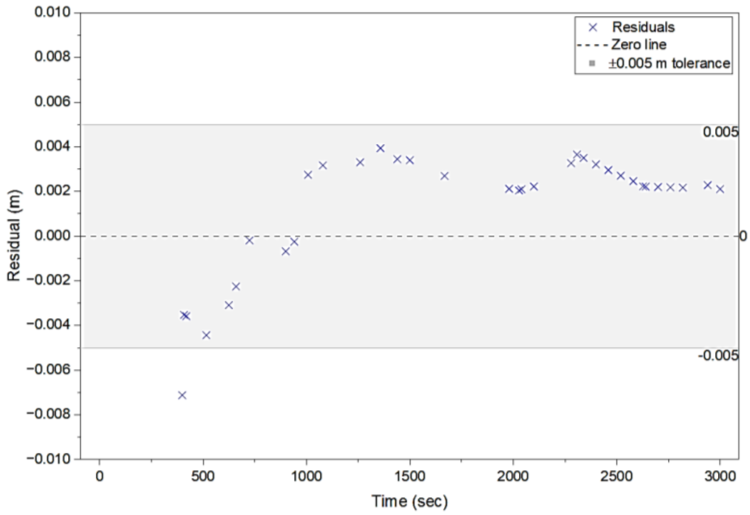

Figure 9. Time Evolution of Residuals

The transition of residual values from negative to positive indicates the shift from initial overprediction to gradual stabilization of the scour process. Overall, residual values remain within ±0.005 m throughout the simulation, indicating good agreement between numerical and experimental results. The remaining discrepancies are attributed to numerical discretization associated with mesh resolution, as well as the simplifications inherent in the turbulence and sediment transport models. A grid independence study was therefore performed to minimize mesh-related effects, and the selected mesh provided the closest agreement with the experimental scour depth.

Numerical Simulation of Pile Groups in A Square Configuration

In this study, Flow-3D was used to simulate sediment scour around a square pile arrangement with three spacing ratios (G/D = 2.5, 3, and 3.5). The numerical setup employed the same boundary conditions and sediment–turbulence models that were validated in the verification stage. The computational channel domain measured 42 m in length, 30 m in width, and 7 m in depth. A pile with a diameter of 1.2 m was located 18 m downstream of the inlet, where a steady inflow velocity of 2 m/s was applied. The 3 m-deep sediment bed consisted of four particle-size classes with median diameters of 0.002, 0.018, 0.022, and 0.024 m. The mesh configuration for each simulation is summarized in

Table 1, where the minimum and maximum cell sizes were 0.12 m and 0.60 m, respectively.

Table 1. Mesh Characteristics for Square Pile Arrangement with Different Spacing Ratios

		Number of piles	Mesh direction	Number of cells	Cell size Min	Cell size Max	Max. adjacent ratio	Max. aspect ratio
Square 2×2 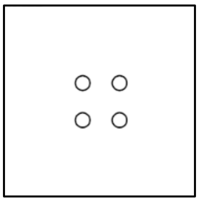	G/D = 2.5	4	x	416	0.12	0.60	1.09	1.00
			y	99	0.12	0.60	1.19	1.00
			z	58	0.12	0.12	1.00	1.00
			Total mesh	2,388,672				
	G/D = 3	4	x	419	0.12	0.60	1.10	1.00
			y	102	0.12	0.60	1.21	1.00
			z	58	0.12	0.12	1.00	1.00
			Total mesh	2,478,804				
	G/D = 3.5	4	x	422	0.12	0.60	1.11	1.00
			y	105	0.12	0.60	1.23	1.00
			z	58	0.12	0.12	1.00	1.00
			Total mesh	2,569,980				
		Number of piles	**Mesh direction**	**Number of cells**	**Cell size Min**	**Cell size Max**	**Max. adjacent ratio**	**Max. aspect ratio**
Square 3×3 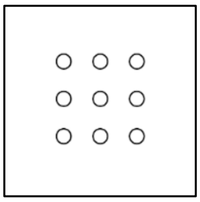	G/D = 2.5	9	x	440	0.12	0.60	1.12	1.00
			y	124	0.12	0.60	1.22	1.00
			z	58	0.12	0.12	1.00	1.00
			Total mesh	3,164,480				
	G/D = 3	9	x	447	0.12	0.60	1.13	1.00
			y	132	0.12	0.60	1.20	1.00
			z	58	0.12	0.12	1.00	1.00
			Total mesh	3,422,232				
	G/D = 3.5	9	x	454	0.12	0.60	1.14	1.00
			y	138	0.12	0.60	1.25	1.00
			z	58	0.12	0.12	1.00	1.00
			Total mesh	3,633,816				
		Number of piles	**Mesh direction**	**Number of cells**	**Cell size Min**	**Cell size Max**	**Max. adjacent ratio**	**Max. aspect ratio**
Square 4×4 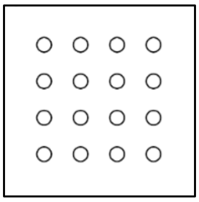	G/D = 2.5	16	x	464	0.12	0.60	1.12	1.00
			y	153	0.12	0.60	1.18	1.00
			z	58	0.12	0.12	1.00	1.00
			Total mesh	4,117,536				
	G/D = 3	16	x	474	0.12	0.60	1.15	1.00
			y	162	0.12	0.60	1.23	1.00
			z	58	0.12	0.12	1.00	1.00
			Total mesh	4,453,704				
	G/D = 3.5	16	x	484	0.12	0.60	1.18	1.00
			y	173	0.12	0.60	1.23	1.00
			z	58	0.12	0.12	1.00	1.00
			Total mesh	4,856,456				

RESULTS AND DISCUSSION

Numerical Simulation of 2×2 (Four Piles) Configuration

The sediment scour around four piles arranged in a square configuration, consisting of two rows and two columns, was simulated. As shown in Figure 10, for a spacing ratio of G/D = 2.5, the maximum local scour depths for piles 1 through 4 are 1.0105 m, 1.0338 m, 0.7954 m, and 0.8435 m, respectively.

For a spacing ratio of G/D = 3, the maximum local scour depths for piles 1 through 4 are 1.0472 m, 1.0553 m, 0.8940 m, and 0.8920 m, respectively. At G/D = 3.5, the corresponding maximum scour depths are 0.9512 m, 0.9657 m, 0.7242 m, and 0.7913 m. The temporal evolution of scour depth, along with the bed-elevation contours around the four-pile square arrangement, is presented in Figures 11 and 12.

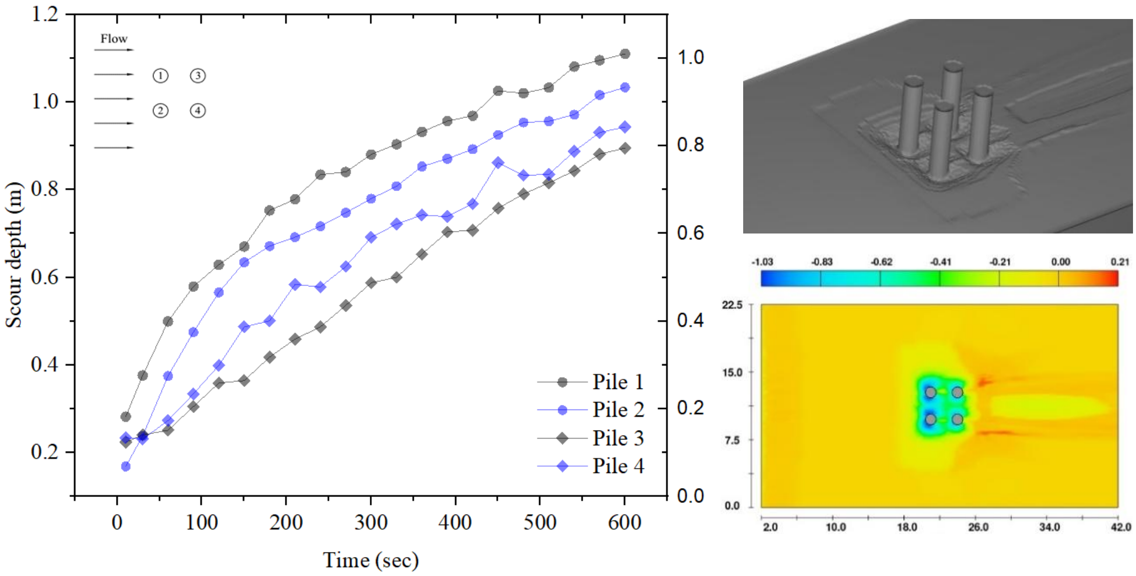

Figure 10. The maximum sediment scour depth around 2×2 (four piles) for G/D = 2.5

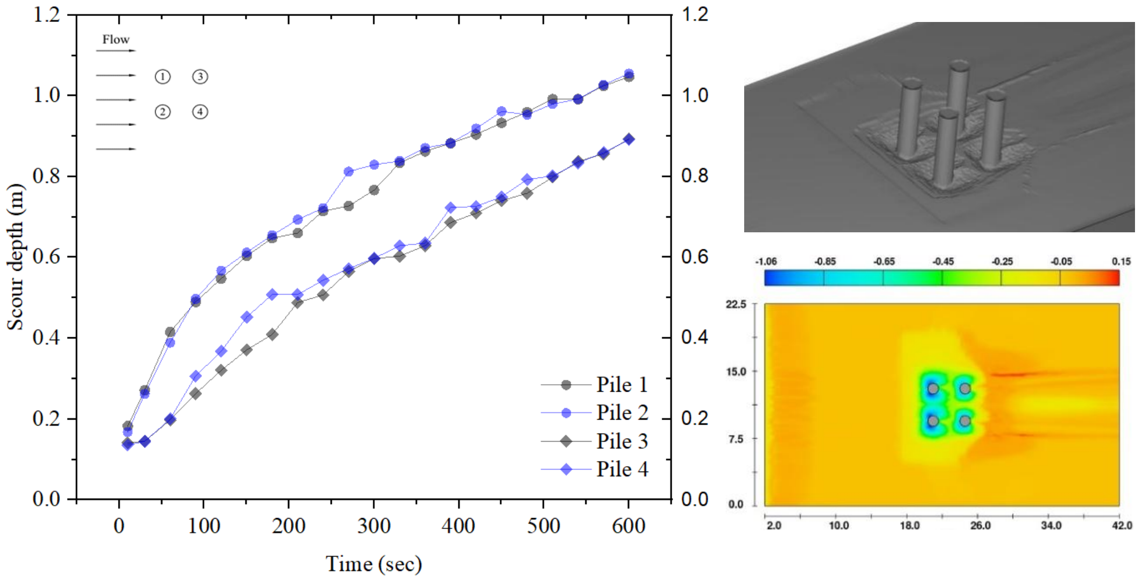

Figure 11. The Maximum Sediment Scour Depth around 2×2 (Four Piles) for G/D = 3

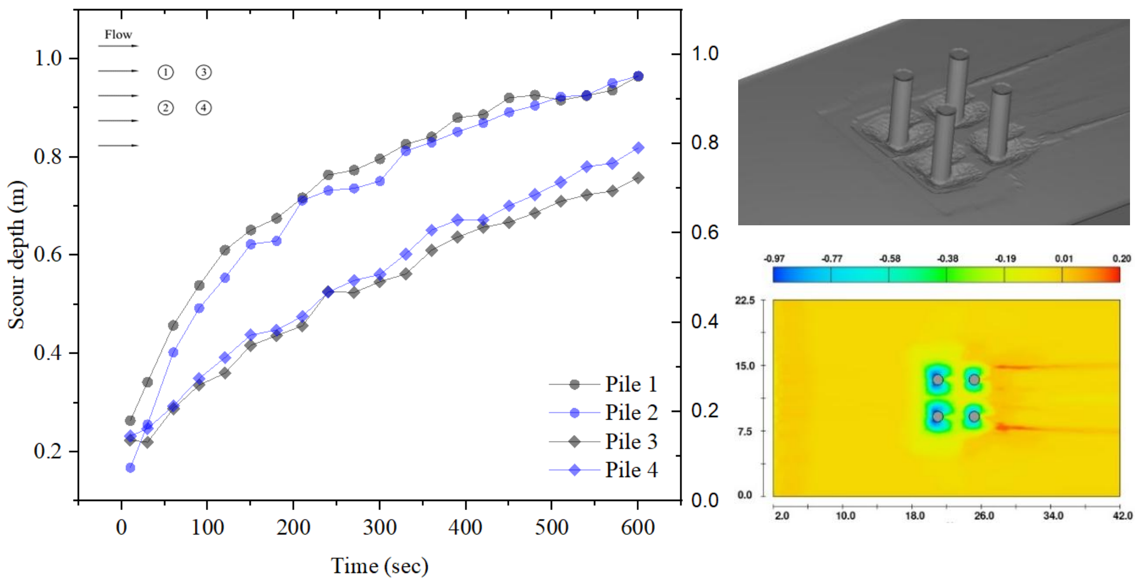

Figure 12. The Maximum Sediment Scour Depth around 2×2 (Four Piles) for G/D = 3.5

Based on the simulation results, the maximum local scour depths and scour-hole contours for piles 1 and 3, as well as for piles 2 and 4, are symmetrical across all G/D values, indicating similar scour patterns on the left and right sides of the pile group. The maximum local scour depth consistently decreases from the front piles to the rear piles due to the sheltering effect generated by the upstream piles, which reduces the flow intensity reaching the downstream piles. When evaluated across different spacing ratios, the average scour depth for both the front and rear piles generally decreases as G/D increases, except at G/D = 3, where the scour is slightly deeper, an observation consistent with the experimental findings of Amini and Solaimani [14]. At larger spacing ratios, the scour holes around individual piles begin to form independently.

However, at the smaller spacing ratio (G/D = 2.5), the scour depth is more dispersed among individual pile locations. This behavior is attributed to strong flow interference between adjacent piles due to their close proximity, which intensifies the interaction between horseshoe vortices and wake vortices. As a result, the flow structure becomes less stable and produces a non-uniform distribution of bed shear stress around the piles, leading to irregular scour depths. In contrast, at larger spacing ratios (G/D = 3 and 3.5), the increased spacing reduces vortex interaction, allowing more stable flow development and more consistent scour patterns. At these spacings, the shielding effect becomes more dominant, resulting in clearly defined differences between upstream and downstream scour depths. Furthermore, at larger spacing ratios, the scour holes around individual piles begin to form more independently.

Numerical Simulation of 3×3 (Nine Piles) Configuration

The sediment scour around nine piles arranged in a three-by-three square configuration was simulated. The maximum local scour depths for each pile are summarized in Table 2, while the temporal evolution of scour depth and the corresponding bed-elevation contours for spacing ratios of G/D of 2.5, 3, and 3.5 are presented in Figures 13 – 15, respectively.

Table 2. Maximum Local Scour Depth around 3×3 Piles

Pile config.	Pile spacing ratio (*G/D*)	Scour depth (m)								
		Pile 1	Pile 2	Pile 3	Pile 4	Pile 5	Pile 6	Pile 7	Pile 8	Pile 9
	2.5	1.0403	1.0813	1.0729	0.8713	0.9282	0.8802	0.6267	0.8158	0.6821
	3	1.0489	1.0872	1.0870	0.9533	1.0886	0.9861	0.7360	0.8337	0.8406
	3.5	0.9922	0.9915	0.9638	0.7704	0.8807	0.7949	0.8067	0.7319	0.7611

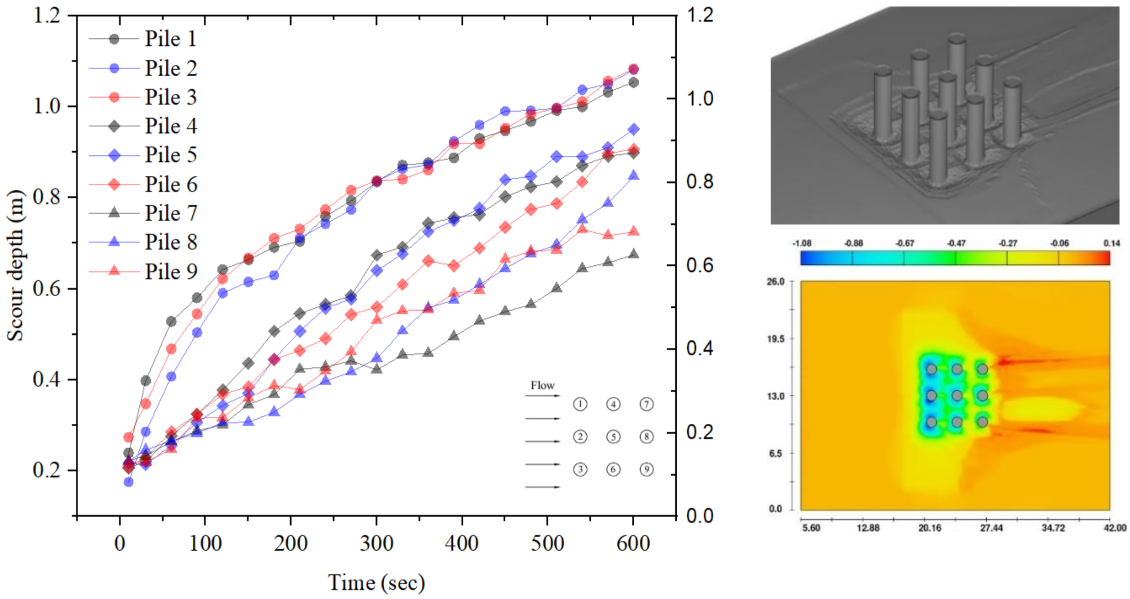

Figure 13. The Maximum Sediment Scour Depth around 3×3 (Nine Piles) for G/D = 2.5

Based on the simulation results, the maximum local scour depths and scour-hole contours for piles 1 through 9 exhibit symmetry with respect to the center pile in the second row across all G/D values, indicating comparable scour depths and scour-hole extents. The maximum scour depth generally decreases from the front row to the rear row due to the sheltering effect produced by the upstream piles. Additionally, the center pile consistently develops slightly deeper scour than the adjacent left and right piles, which can be attributed to its position and the intensified flow interference among surrounding piles. An exception occurs at G/D = 3.5, where the scour around each pile begins to develop independently. These trends are consistent with the experimental findings reported by Wang et al. [9]. When compared across different pile spacing ratios, the average scour depth for the front and middle piles generally decreases as G/D increases, with the exception of G/D = 3, which produces the greatest scour depth. In contrast, the rear piles show an opposite trend, where the average scour depth increases with larger spacing ratios, although the deepest scour still occurs at G/D = 3. As the spacing continues to increase, the scour depths and scour-hole areas around individual piles begin to develop independently and eventually resemble those of isolated single piles.

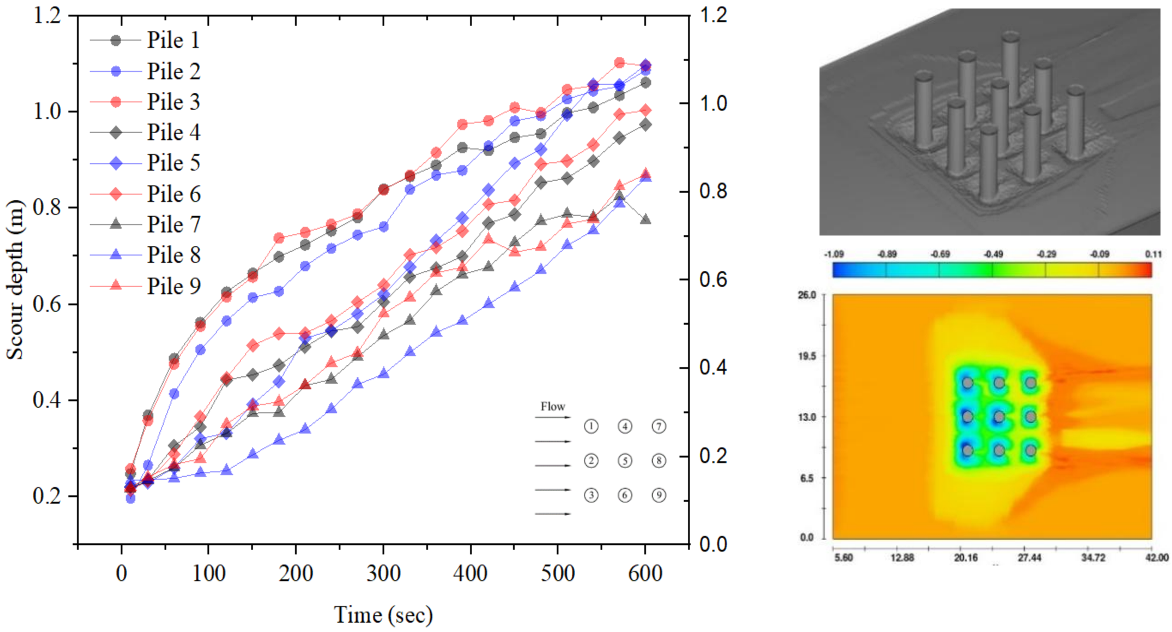

Figure 14. The Maximum Sediment Scour Depth around 3×3 (Nine Piles) for G/D = 3

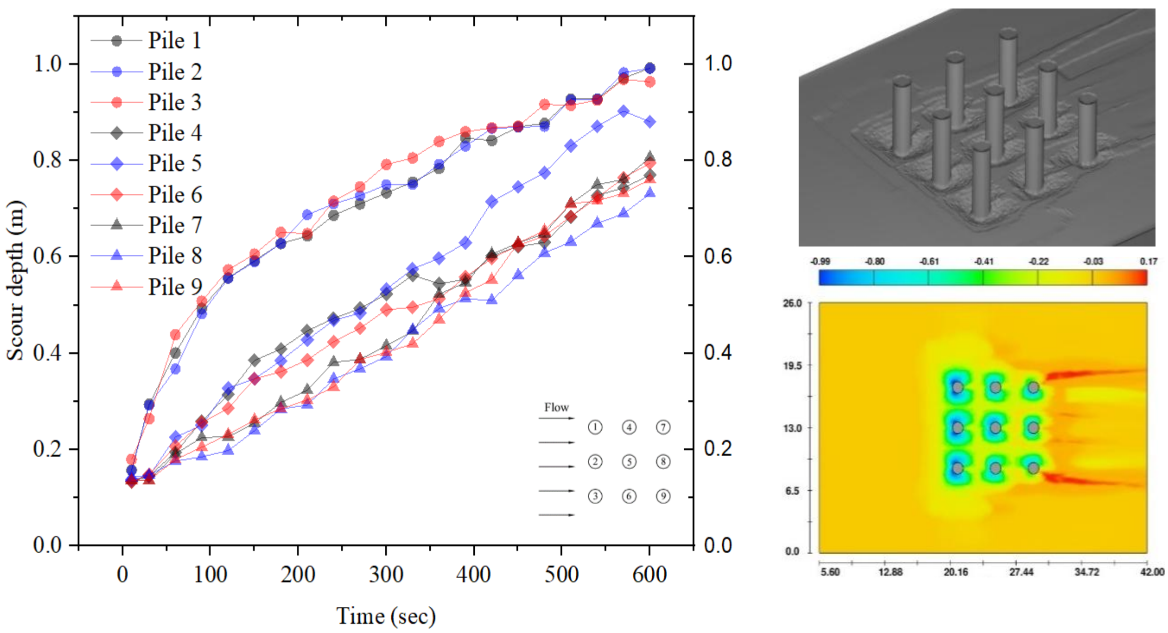

Figure 15. The Maximum Sediment Scour Depth around 3×3 (Nine Piles) for G/D = 3.5

Numerical Simulation of 4×4 (Sixteen Piles) Configuration

The sediment scour around sixteen piles arranged in a four-by-four square configuration was simulated. The maximum local scour depths for each pile are listed in Table 3, while the temporal evolution of scour depth and the associated bed-elevation contours for spacing ratios of G/D of 2.5, 3, and 3.5 are presented in Figures 16 – 18, respectively.

Table 3. Maximum Local Scour Depth around 4×4 Piles

Pile config.	Pile spacing ratio (*G/D*)	Scour depth (m)							
		Pile 1	**Pile 2**	**Pile 3**	**Pile 4**	**Pile 5**	**Pile 6**	**Pile 7**	**Pile 8**
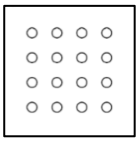	2.5	0.9182	0.9667	0.9951	0.9529	0.7252	0.7567	0.7740	0.7339
	3	1.0142	1.0504	0.9986	0.9904	0.7998	0.9273	0.9217	0.7994
	3.5	1.1155	1.0520	1.0759	1.1040	0.9751	1.0947	1.1131	0.9754
	(*G/D*)	**Pile 9**	**Pile 10**	**Pile 11**	**Pile 12**	**Pile 13**	**Pile 14**	**Pile 15**	**Pile 16**
	2.5	0.4838	0.6263	0.6295	0.4881	0.5539	0.6242	0.5780	0.4062
	3	0.6604	0.8064	0.8034	0.7322	0.7384	0.8583	0.7259	0.8963
	3.5	0.9224	1.0752	0.9710	0.8836	1.1319	1.1126	1.0788	0.8733

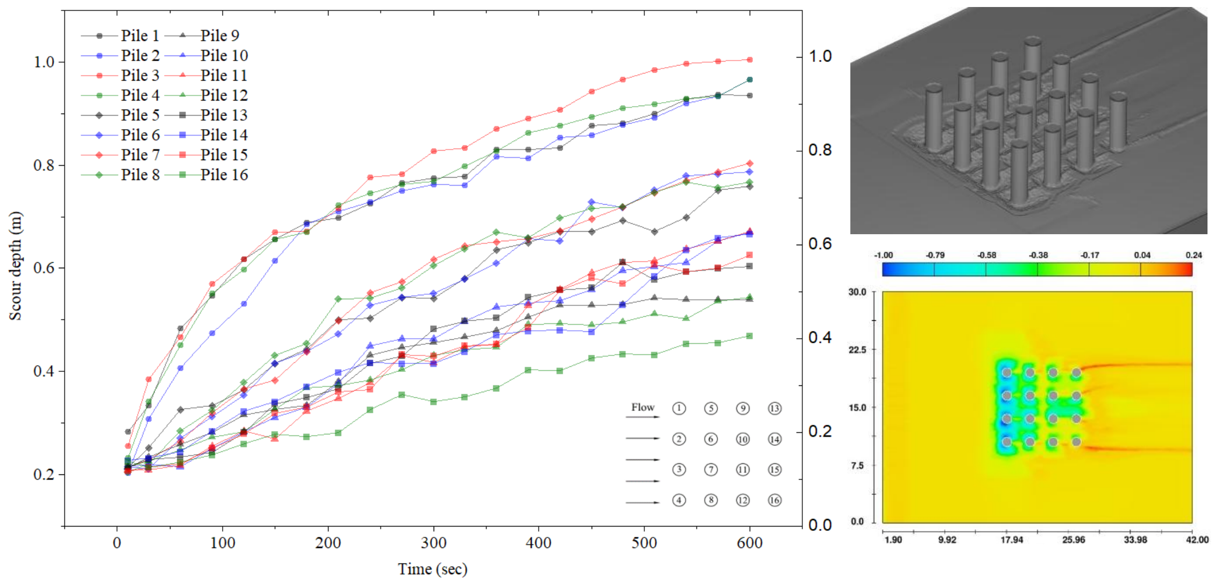

Figure 16. The Maximum Sediment Scour Depth around 4×4 (Sixteen Piles) for G/D = 2.5

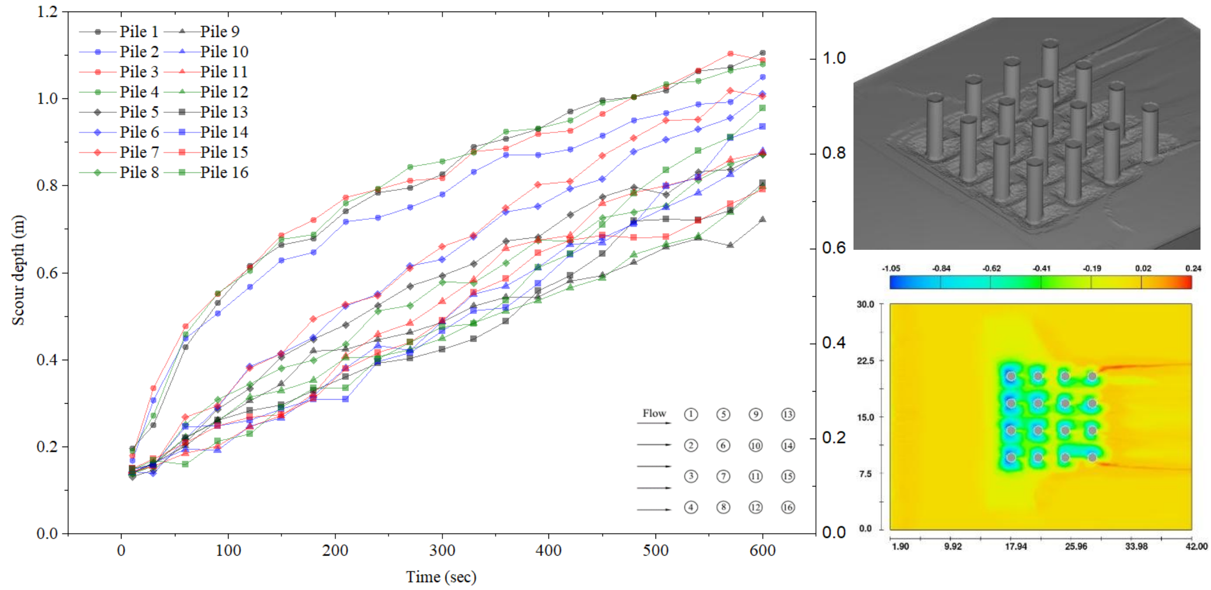

Figure 17. The Maximum Sediment Scour Depth around 4×4 (Sixteen Piles) for G/D = 3

Based on the simulation results, the maximum local scour depths and scour-hole contours for piles 1 through 16 exhibit symmetry about the center of the pile group across all G/D values, indicating comparable scour patterns and scour-hole extents. The maximum scour depth generally decreases from the front rows to the downstream rows due to the sheltering effect of the upstream piles, although several piles in the fourth column show deeper scour than expected. The central pile also develops slightly greater scour compared with the adjacent left and right piles, which can be attributed to its position and the intensified flow interaction among neighboring piles. When evaluated across different spacing ratios, the average scour depth for each column increases as G/D becomes larger. Ultimately, as the spacing increases, the scour depth and scour-hole region around each pile begin to form independently and gradually approach those characteristic of a single isolated pile.

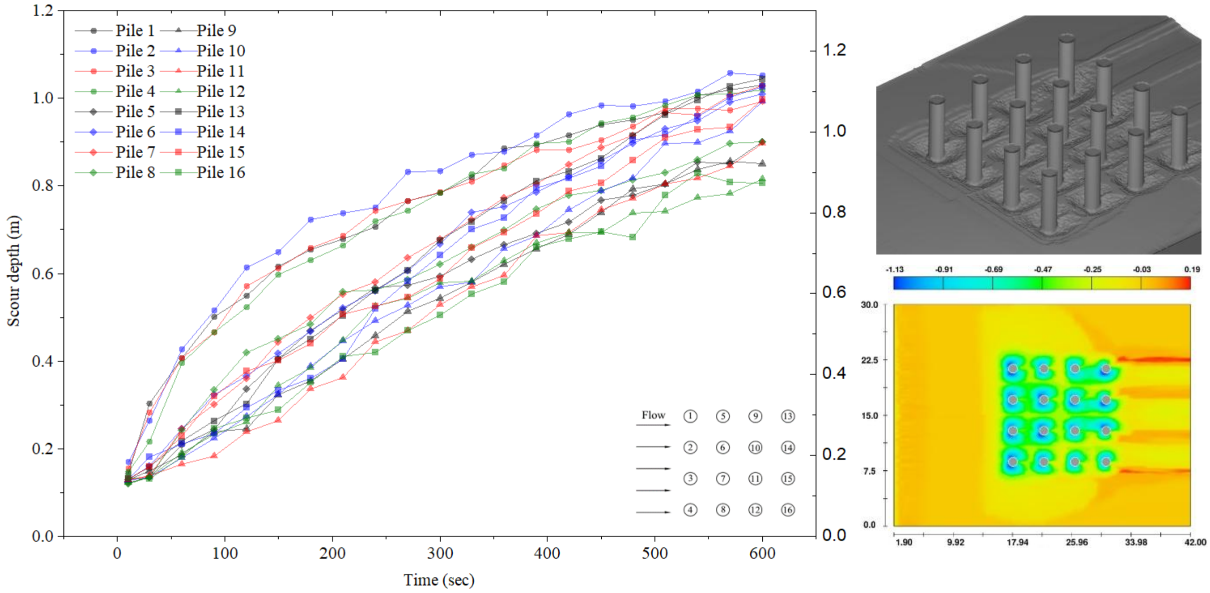

Figure 18. The Maximum Sediment Scour Depth around 4×4 (Sixteen Piles) for G/D = 3.5

The scour patterns observed in Figures 16–18 indicate that upstream piles exhibit relatively consistent scour depths across different configurations. This behavior is attributed to direct exposure to the incoming flow, which generates stable downflow and horseshoe vortices responsible for initiating scour. In contrast, downstream piles exhibit more variable scour depths, such as the differences observed between pile 7 and pile 8. This variability is caused by wake interference and turbulent flow interactions generated by upstream piles, resulting in non-uniform bed shear stress distribution.

The similarity in scour patterns between the 3×3 and 4×4 configurations suggests that flow shielding becomes dominant after several upstream rows, reducing the available flow energy reaching downstream piles. Consequently, additional downstream rows contribute less significantly to changes in scour behavior.

In addition, the potential influence of boundary conditions on the predicted scour patterns was carefully evaluated. The computational domain was designed with sufficient upstream and downstream lengths to ensure fully developed flow conditions before the pile group and to allow wake vortices and sediment transport processes to dissipate naturally without interference from the outlet boundary [15,16]. As a result, the primary scour features occur within the central region of the domain, far from the boundaries.

No abnormal scour concentration or flow distortion was observed near the upstream or downstream boundaries, indicating that the selected domain size effectively minimizes boundary-induced effects. Similar approaches adopted by Omara and Tawfik [17] in defining sufficiently large computational domains have been adopted in previous numerical studies to reduce artificial boundary influence and ensure reliable prediction of local scour processes.

CONCLUSIONS

This study numerically investigated the development of local scour around square pile groups consisting of 2×2, 3×3, and 4×4 configurations under three spacing ratios (G/D = 2.5, 3, 3.5) using the CFD software Flow-3D. The numerical model incorporated the RANS equations with the RNG k–ε turbulence closure, the FAVOR method for geometric representation, and the Van Rijn sediment transport formulation [10]. Model verification against experimental data for a single pile, together with a grid independence study, demonstrated that the selected mesh provides mesh-independent predictions with good agreement to the measured scour depth. The remaining differences between the numerical and experimental results are primarily associated with numerical discretization and modeling assumptions rather than a predefined error tolerance.

The simulation results show that scour development around square pile groups is governed by a combination of turbulent flow structures, pile–pile interactions, and spacing effects. For all configurations, scour-hole contours and maximum local scour depths exhibited clear symmetry relative to the geometric center of the pile group. The scour consistently decreased from the upstream to downstream rows due to the sheltering effect, although localized deviations appeared in the downstream columns of larger (4×4) groups. The center piles tended to experience slightly deeper scour than adjacent piles owing to intensified flow interference.

Pile spacing played a significant role in the magnitude and spatial distribution of scour. Smaller spacing ratios generated stronger hydrodynamic interference and produced deeper, more connected scour holes, while larger spacing ratios reduced interference, allowing scour holes to develop independently and approach patterns characteristic of isolated single piles. Although the general trend indicated decreasing scour depth with increasing spacing, the spacing ratio G/D = 3 produced slightly deeper scour across several configurations, consistent with previously reported experimental observations.

Overall, the findings demonstrate that Flow-3D provides a robust and efficient tool for simulating complex flow–sediment interactions around pile groups. The insights obtained from this study contribute to a more comprehensive understanding of scour mechanisms in square pile arrangements and offer practical guidance for optimizing pile spacing and configuration in the design of bridge piers and offshore foundations to mitigate scour-induced risks.

ACKNOWLEDGEMENTS

The authors have no acknowledgements to declare.

REFERENCES

1. Józefiak, K., Zbiciak, A., Mašlakowski, M., and Piotrowski, T., Numerical Modelling and Bearing Capacity Analysis of Pile Foundation, *Procedia Enginering*, 111, 2015, pp. 356–363.
2. Qi, W.G., Li, Y.X., Xu, K., and Gao, F.P., Physical Modelling of Local Scour at Twin Piles under Combined Waves and Current, *Coastal Engineering*, 143, 2019, pp. 63–75.
3. LeBeau, K.H. and Wadia-Fascetti, S.J., Fault Tree Analysis of Schoharie Creek Bridge Collapse, *Journal of Performance of Constructed Facilities*, 21(4), 2007, pp. 320–326.
4. Hong, J.H., Chiew, Y.M., Lu, J.Y., Lai, J.S., and Lin, Y.B., Houfeng Bridge Failure in Taiwan, *Journal of Hydraulic Engineering,* 138(2), 2012, pp. 186–198.
5. Ghaderi, A. and Abbasi, S., CFD Simulation of Local Scouring around Airfoil-Shaped Bridge Piers with and without Collar, *Sādhanā*, 44(10), 2019, pp. 1 – 12.
6. Zhang, Q., Zhou, X.L., and Wang, J.H., Numerical Investigation of Local Scour around Three Adjacent Piles with Different Arrangements under Current, *Ocean Engineering,* 142, 2017, pp. 625–638.
7. Puspasari, A.D. and Tang, J.H., Review on the Numerical Simulation Model of Scouring around Bridge Pier by using Flow-3D Software, *Journal of Civil Engineering, Planning and Design,* 3(2), 2024, pp. 79–92.
8. Abdeldayem, A.W., Elsaeed, G.H., and Ghareeb, A.A., The Effect of Pile Group Arrangements on Local Scour using Numerical Models, *Advances in Natural and Applied Sciences,* 5(2), 2011, pp. 141–146.
9. Wang, C., Liang, F., and Yu, X., Experimental and Numerical Investigations on the Performance of Sacrificial Piles in Reducing Local Scour around Pile Groups, *Natural Hazards*, 85, 2016, pp. 1417–1435.
10. Van Rijn, L.C. Sediment Transport, Part I: Bed Load Transport, *Journal of Hydraulic Engineering*, ASCE, 110(10), 1984, pp. 1431–1456.
11. Hyperinfo Corporation, *Flow-3D v11.2 User Manual*, Hyperinfo Corporation, Taiwan, 2016.
12. Khosronejad, A., Kang, S., and Sotiropoulos, F., Experimental and Computational Investigation of Local Scour around Bridge Piers, *Advances in Water Resources*, 37, 2012, pp. 73–85.
13. Tang, J.H. and Puspasari, A.D., Numerical Simulation of Local Scour around Three Cylindrical Piles in a Tandem Arrangement, *Water,* 13(24), 2021, pp. 1–19.
14. Amini, A. and Solaimani, N. The Effects of Uniform and Nonuniform Pile Spacing Variations on Local Scour at Pile Groups, *Marine Georesources and Geotechnology*, 36(7), 2018, pp. 861–866.
15. Cengel, Y.A. and Cimbala, J.M., *Fluid Mechanics: Fundamentals and Applications*, McGraw-Hill, New York, 2014.
16. Bonakdari, H., Lipeme-Kouyi, G., and Lal Asawa, G., Developing Turbulent Flows in Rectangular Channels : A Parametric Study, *Journal of Applied Research in Water and Wastewater,* 2, 2014, pp. 51–56.
17. Omara, H. and Tawfik, A., Numerical Study of Local Scour around Bridge Piers, *Proceedings of the 9th International Conference on Environmental Science and Development (ICESD 2019),* Paris, France, February 7-9, 2018, pp. 1-8.